Piezoelectric ion gated organic electrochemical transistors for efficient vibration sensing and on-site amplification

Sohail, Linta; Drakopoulou, Sofia; Costa, Tiago L.; Spyropoulos, George D.

Important note
To cite this publication, please use the final published version (if applicable).
Please check the document version above.

Piezoelectric ion gated organic electrochemical transistors for efficient vibration sensing and on-site amplification

Check for updates

Linta Sohail[1], Sofia Drakopoulou[1], Tiago L. Costa[2] & George D. Spyropoulos[1] ✉

Accurate detection of physiological vibrations is vital for monitoring health and enabling sensory feedback in bioelectronics. Current technologies often suffer from low signal-to-noise ratios (SNR), bulkiness, and the need for external amplification. Here, we introduce piezoelectric internal ion-gated organic electrochemical transistors (Piezo-IGTs), which efficiently convert mechanical vibrations into amplified electrical signals. These devices integrate laminated P(VDF-TrFE) microfiber films as the gate atop the transistor channel, generating voltage upon deformation to modulate mobile ions in the conducting polymer. Fabricated via sequential deposition and lamination, Piezo-IGTs achieve high fill factors and efficient on-site amplification, improving SNR over standalone piezoelectric films. They operate near 0 V gate voltage, enabling low-power performance. We validate their functionality in mechanomyography, speech recognition, and mechanocardiography using microscale Piezo-IGTs. This self-contained, flexible architecture demonstrates promise for integration into implantable and wearable systems, offering real-time, high-fidelity acquisition of bio-mechanical signals in next-generation health monitoring and neuroprosthetic applications.

Neural interfaces have revolutionized our understanding of neural dynamics during complex physiological processes, offering transformative potential for treating drug-resistant neuropsychiatric diseases (e.g. epilepsy[1,2]) and sensory dysfunction (e.g. hearing loss[3,4]). Furthermore, they hold immense promise for neurorehabilitation, including delivering targeted auditory stimulation[5–7], providing sensory feedback in neural prosthetics[8], and acquiring physiological data to deepen our understanding of physiological mechanisms[9–12]. However, current technologies face critical challenges that limit their effectiveness and integration into advanced bioelectronics. These include: (i) non-flexible interfaces[13], which can lead to rejection or degradation; (ii) bulky and power-consuming external components, restricting miniaturization and portability; and (iii) low signal-to-noise ratio (SNR), which hampers the accurate acquisition of biologically relevant signals. Addressing these limitations requires the development of next-generation devices that are fully implantable, self-powered, and capable of seamlessly interfacing with biological systems[13].

Devices that respond to mechanical deformation are especially promising, as they can establish a communication pathway by translating mechanical stimuli, such as touch, sound etc., from the environment or a part of the body into electrical signals -the fundamental language of neuronal communication. Selecting materials with optimal response properties is crucial for such devices. Memory alloys and piezoelectric materials are most used to achieve this[14,15]. Piezoelectric materials possess the unique ability to generate electric charge in response to mechanical stress (e.g. caused by vibrations) without requiring additional components[6,7]. Moreover, sensors made of piezoelectric polymers stand out for their flexibility, sensitivity, and high-frequency selectivity[16]. Their favorable form factors allow the fabrication of diverse geometries with freedom of shape and conformability, making them suitable for demanding topographies such as that of the inner cochlea[17]. Most piezoelectric devices are traditionally based on lead-zirconate-titanate (PZT), aluminum nitride, and polyvinylidene fluoride (PVDF)[14,16,18]. However, both PZT and aluminum nitride face limitations, particularly in terms of biocompatibility and stiffness[19]. In contrast, PVDF[20] and its copolymer poly(vinylidene fluoride-tri-fluoroethylene) (PVDF-TrFE)[16] offer high piezoelectricity along with good chemical stability, ease of processing, and favorable mechanical

[1]Department of Information Technology, Faculty of Engineering and Architecture, Ghent University, Technologiepark Zwijnaarde 126, 9052 Zwijnaarde, Belgium.
[2]Bioelectronics section, Department of Microelectronics, Delft University of Technology, 2628 CD Delft, The Netherlands.
✉e-mail: Georgios.Spyropoulos@UGent.be

properties[18,21,22]. Among the various methods used to process PVDF and PVDF-TrFE, electrospinning has gained significant attention due to its simplicity and ability to produce piezoelectric fibers with up to five times higher selectivity for acoustic signals[19]. The piezoelectric response of the electrospun fibrous films can be fine-tuned by modifying the fiber geometry and morphology[19]. In addition, electrospinning exerts substantial stretching forces on the piezoelectric material, which leads to the formation of self-poled fibrous films[23,24].

PVDF fibrous film-based flexible sensors have been extensively studied for detecting minute pressure and motion changes in both animals and humans[25–27]. These sensors are sensitive to movements such as muscle contractions and breathing. For example, a mechanomyography (MMG) sensor made from PVDF nanofibers was developed to monitor lower limb movements[28]. However, the signals generated by the MMG were weak, requiring amplification and filtration for effective signal processing[28]. Similarly, PVDF-TrFE/Nanoclay sensors can capture body vibrations, much like a traditional stethoscope[29]. These sensors require an acquisition system that includes an amplifier, filter, and analog-to-digital converter. To enhance piezoelectric performance, PVDF nanocomposite-based nanogenerators have been used to detect movements in the elbow and knee, yielding a high output voltage[20,30]. Advances in PVDF fibers have also been explored for their potential application in cochlear implants. PVDF fiber-based acoustic circular sensors were fabricated and tested for their resonance frequencies, producing voltage outputs of $1-17$ mV at frequencies ranging from 100 to 400 Hz[19].

While flexible piezoelectric sensors show potential for external, part-free implants, their inefficient displacement-to-electric transduction for neuron stimulation still requires additional amplification and processing, often relying on conventional components. These components, typically made from silicon-based electronics, suffer from mechanical mismatch and poor biocompatibility, necessitating bulky encapsulations[13,31]. To improve

signal amplification, researchers have explored integrating piezoelectric films with organic electrochemical transistors (OECTs)[32–34]. In these designs, however, the piezoelectric film typically functions as a separate gate, transferring signals to the OECT via external cables[35]. This configuration is inherently prone to impedance mismatches and signal losses, resulting in suboptimal performance. Moreover, these architectures often suffer from poor fill factors, limiting the utilization of the active piezoelectric area. This, coupled with constraints in form factor, hinders their miniaturization and broader applicability. As a result, these devices perform suboptimally at the interface with biological tissues, reducing their effectiveness for implantable applications and undermining their intended purpose[36].

To address these challenges, we introduce a new generation of self-contained, flexible, and soft piezoelectric internal ion-gated organic electrochemical transistor architecture (Piezo-IGT) that eliminates the need for external connections and enables efficient transduction of mechanical vibrations into electrical signal with on-site amplification (Fig. 1A). This system is based on internal ion-gated organic electrochemical transistors (IGTs)[37,38] which ensure high gain-bandwidth product (several orders of magnitude above that of other ion-based transistors) and poly(vinylidene fluoride-trifluoroethylene) (PVDF-TrFE) films as the gate material. Unlike conventional OECT-based designs, Piezo-IGTs integrate the piezoelectric gate, ionic membrane, and IGT-channel into a single, self-contained system (Fig. 1B). This seamless integration, achieved through sequential deposition and lamination techniques, minimizes alignment issues and eliminates the impedance mismatches and signal losses associated with external wiring. The optimized architecture achieves a high fill factor, ensuring maximum utilization of the active piezoelectric area and significantly improving transduction efficiency. By incorporating a flexible transistor gain-stage directly into the flexible piezoelectric sensor, we achieve simultaneous full flexibility of both the sensor and front-end electronics, along with an enhanced SNR, a level of performance that traditionally required rigid,

Fig. 1 | Piezo-IGTs enable high-SNR flexible piezoelectric transduction. A Schematic comparison of different signal transduction architectures: (i) standalone piezoelectric element without a pre-amplifier picks up a signal but suffer from low SNR (ii) piezoelectric element with a conventional silicon-based front-end amplifier improves SNR but compromise system flexibility. (iii) Piezo-IGTs integrate piezoelectric sensing and front-end amplification enabling high SNR into a flexible platform. S is the signal from a pressure source, N denotes the input noise (background vibration noise, sensor and front-end amplifier, if present), aS and aN correspond to the amplified signals and N_{BE} is the back-end noise. All signals are amplitude-normalized for illustration purposes. **B** Schematic illustration depicting the fundamental building blocks of Piezo-IGT (upper) and an overview of potential applications in various mechan-oresponsive bioelectronics systems (lower). Mechanical vibrations deform the piezoelectric element, generating voltage that modulates the transistor's channel current via ionic gating, resulting in amplified output signals. Piezo-IGT architecture enables the capture of high-quality signals from mechanocardiography (MCG), mechan-omyography (MMG), speech recognition systems, electronic skin and next-generation auditory prostheses systems.
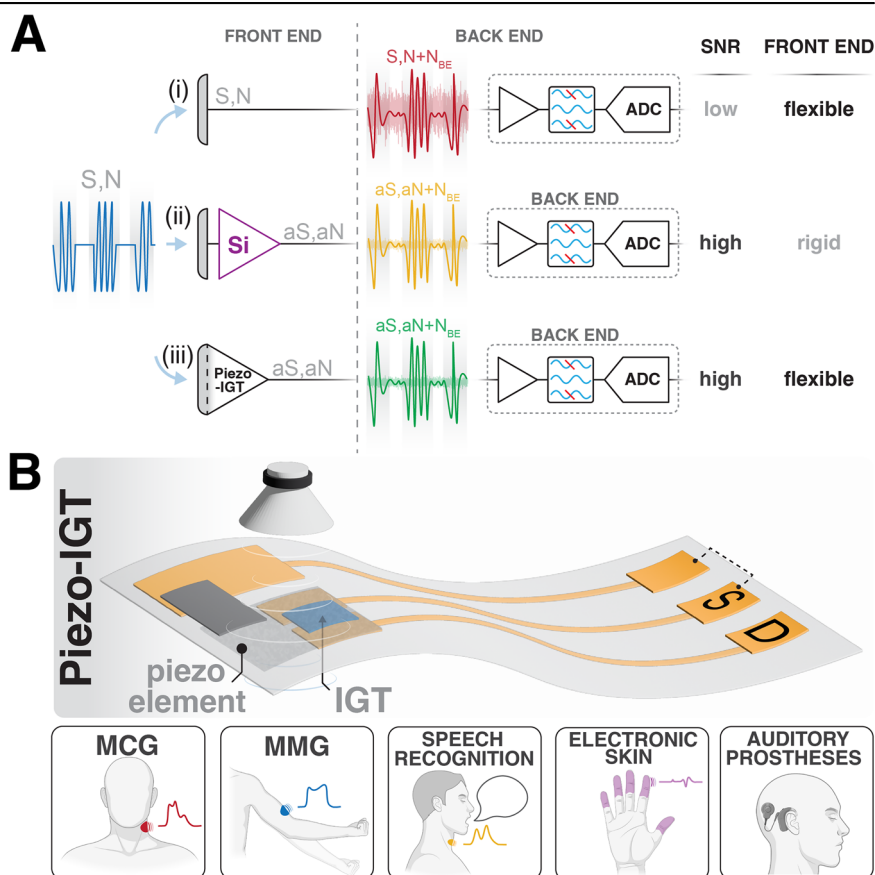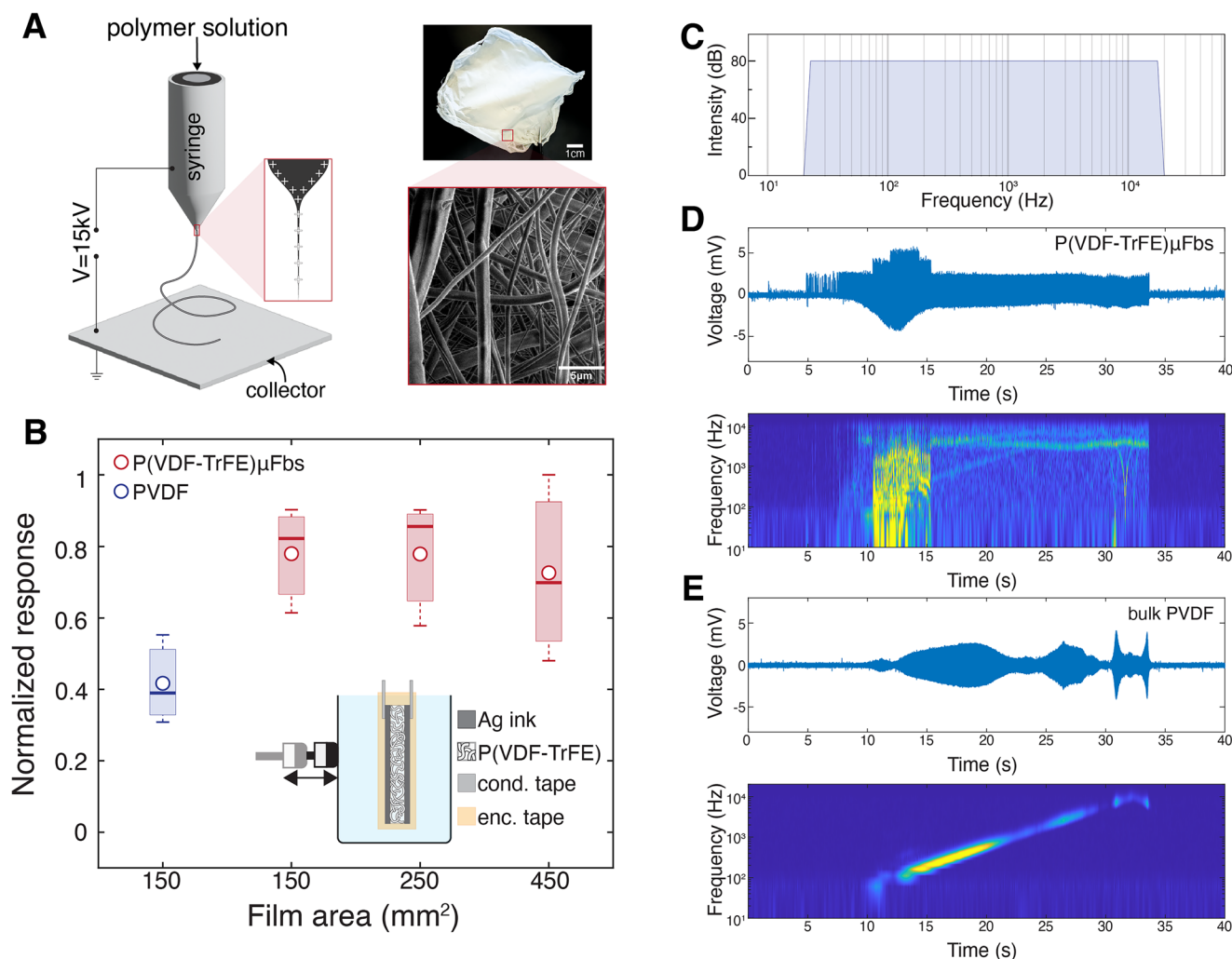
Fig. 2 | PVDF films enable highly sensitive and selective piezoelectric transduction. A Schematic illustration of electrospinning setup, where a 15KV is applied between the needle and the collector, forming a Taylor cone at the tip of syringe with polymeric solution (inset). This results in the formation of a fibrous film on the collector (top right). Scanning electron microscopy (SEM) image displays randomly aligned fibers in the P(VDF-TrFE) μFb film (bottom right). **B** Normalized voltage response of bulk PVDF film (thickness: 52 μm, blue) as compared to P(VDF-TrFE) μFb films (feed-rate: 5 ml/h, thickness: 52 μm, red), under similar tapping conditions (100 Hz). A schematic illustration of the setup used for the characterization of the films is shown (inset), including a container filled with deionized water (DI) and a tapping machine. **C** Sound wave frequency sweep in the range of 20–20000 Hz (5–35 s) maintained at constant intensity of 80 dB, used to characterize the response of bulk PVDF and P(VDF-TrFE) μFb films. **D** Response of μFbs (feed-rate: 5 ml/h, thickness: 52 μm) to the sound wave frequency sweep shown in (**C**) (top) and the corresponding time-frequency spectrogram (bottom). **E** Response of bulk PVDF film (thickness: 52 μm) to the sound wave frequency sweep shown in (**C**) (top) and the corresponding time-frequency spectrogram (bottom).

silicon-based electronics. The SNR is enhanced by integrating a gain-stage directly at the interface with the piezoelectric sensor, which mitigates potential electromagnetic interference picked up by interconnections between sensor and back-end electronics, as well as highly attenuates the contribution of the back-end electronics to the input referred noise at the sensor terminals. Mechanical deformation of the laminated piezoelectric films generates sufficient voltage to dope and de-dope the polymeric channel of the IGT, which shows maximum transconductance around zero gate voltage ($V_G \sim 0$) eliminating the need for external gate biasing. This results in fast, amplified piezoelectric transduction with a significantly improved SNR compared to standalone piezoelectric films, bypassing the need for additional signal processing. The great form factor and morphology of P(VDF-TrFE) μFb films further enhance the sensitivity of Piezo-IGTs to high frequency vibrations, aligning with the biologically relevant frequency range. We validated the performance of Piezo-IGTs by capturing high-quality, amplified signals from various sources of mechanical vibrations, including mechanomyography (MMG), speech recognition, and mechanocardiography (MCG). Piezo-IGTs possess all the key properties required

for integration into bioelectronic systems enabling the acquisition, amplification, and processing of vibrational signals from biological and environmental sources (Fig. 1B).

Results

PVDF films enable highly sensitive and selective piezoelectric transduction

We employed electrospinning to fabricate randomly oriented P(VDF-TrFE) microfibers (μFbs). This configuration was selected based on previous studies, which suggest that randomly oriented fibers exhibit a higher piezoelectric response compared to aligned fibers[19]. First, we explored the relationship between the structure, size, and morphology of P(VDF-TrFE) μFb films and their effects on piezoelectric properties. Additionally, we compared these characteristics to those of bulk PVDF films to assess performance differences. Maintaining a constant voltage and needle-to-collector distance (Fig. 2A), we systematically varied the feed rates (3, 4, 5, and 6 ml/h), achieving control over fiber diameters within the 1–3 μm range. The resulting material is a white, porous μFbs-based film (Fig. 2A, upper

right), with its thickness directly influenced by the duration of electro-spinning process. To ensure consistency across all samples, the electro-spinning duration was kept constant at approximately 60 min for each film. Scanning electron microscopy (SEM) images (Fig. 2A, lower right, Supplementary Fig. S7) confirmed the surface morphology and surface porosity of the PVDF μFb films, revealing a fibrous network. In contrast, commercial bulk PVDF films display a smooth, uniform surface[39]. The increased surface roughness of the μFb films suggests a larger surface area, which may contribute to enhanced piezoelectric properties for specific frequency bands[40]. To further correlate morphology with mechanical performance, stress–strain test was performed on bulk PVDF and P(VDF-TrFE) μFbs films. The PVDF-TrFE μFbs exhibited a highly stretchable behavior, with strain values exceeding 250% before fracture. The calculated Young's modulus for the microfiber mat was approximately 0.73 MPa, with a fracture stress of 1.61 MPa. In contrast, the bulk PVDF film displayed a significantly stiffer response, characterized by a Young's modulus of 13.91 MPa and minimal strain capacity (Supplementary Fig. S10).

Efficient charge extraction from the piezoelectric μFb films requires the deposition of thin conductive layers on either side of the film, a challenging task due to film's porosity. These layers must provide sufficient electronic conductivity without causing short circuits. The degree of overlap between these conductive layers defines the active area of the P(VDF-TrFE) μFb films responsible for charge generation. We evaluated a range of commercially available materials and lab-synthesized conductive hydrogels as charge extraction contacts by immersing encapsulated PVDF films in deionized (DI) water and applying controlled surface taps at 100 Hz using a custom Arduino-based tapping device (Fig. 2B, inset and Supplementary Fig. S5). Drawing inspiration from the structure of the middle ear and traveling wave theory[41], the tapping motion on the outer surface generated vibrations, which were transmitted through the glass, into the liquid, and finally to the PVDF films, resulting in a measurable voltage response. Among the various charge extraction layers tested, the P(VDF-TrFE) fibrous films with screen-printed Ag ink contacts (average sheet resistance 4.37 Ω/sq)[42] exhibited the highest piezoelectric response, producing approximately 80 mV (Supplementary Fig. S5). This superior performance can be attributed to the hydrophilic nature and viscosity[43] of Ag ink, which spreads and conforms well over the porous μFb structure. Further annealing (80 °C) enhances the stability and wettability of μFb film. Other materials, such as conductive hydrogels (CH) based on PEDOT:PSS and DMSO, showed lower output (~20 mV) potentially due to insufficient contact with the porous μFb surface (Supplementary Fig. S5). While the inclusion of anisotropic conductive film (ACF) as a sandwich layer slightly improved the contact, it compromised the flexibility of the μFb film. Although alternatives like carbon paint and conductive graphite paste provided adequate coatings, their high resistance 10–100 s kΩ) impeded signal quality. Notably, the optimized Ag ink μFb films outperformed commercially available bulk PVDF films (52 μm thickness) by 40% in piezoelectric response for similar film areas (150 mm²) (Fig. 2B). This improvement can be attributed to the micro-structured morphology and higher elastic modulus of the fibrous films, which allow for greater deformation under vibrations. However, P(VDF-TrFE) μFb films with larger areas (area 200 mm² and 400 mm²) did not show further improvement in performance. While the larger area resulted in higher output, it also introduced greater variability, likely due to defects in the electrode layers. This increased variability is evident in the larger error bars observed.

Frequency response tests revealed further distinctions between μFb and bulk PVDF films when subjected to a frequency sweep from 20 to 20,000 Hz (Fig. 2C–E). The sweep duration was set to increase linearly over a period of 30 s, beginning at 5 s and concluding at 35 s. The sound pressure level (SPL) was maintained at 80 dB throughout the test to ensure consistency in acoustic excitation. The power spectrogram and voltage response of the fibrous films (20 mm diameter) revealed significant deformations at frequencies below 1000 Hz, with diminished variation in response at higher frequencies and peak-to-peak maximum at ~150 Hz (Fig. 2D, Supplementary Fig. S6). The μFb spectrogram exhibited a broad power distribution

across the frequency range, indicating sensitivity to multiple frequency components. In contrast, bulk PVDF films showed a more linear spectrogram with prominent peaks near 10 kHz, corresponding to their high resonance frequency (Fig. 2D, E, and Supplementary Fig. S6). The unique characteristics suggest that both μFb and bulk films are well-suited for complementary use in frequency-specific applications.

Piezo-IGT as an efficient piezoelectric transducer and amplifier

Next, we integrated P(VDF-TrFE) μFbs with IGTs to develop Piezo-IGTs, designed to amplify on-site piezoelectric activity. These Piezo-IGTs consist of a conducting polymer-based channel, an ion membrane, and a laminated P(VDF-TrFE) μFbs film (Fig. 3A top). The channel is composed of poly(3,4-ethylenedioxythiophene) polystyrene sulfonate (PEDOT:PSS), enriched with the hydrophilic sugar alcohol D-sorbitol to facilitate water molecule uptake and ensure high gain bandwidth product[37,38]. To ensure efficient ionic conduction between the μFbs layer and the channel, we introduced a chitosan: glycerol based ion membrane (IM) as an intermediate layer[44] (Fig. 3A top and Supplementary Fig. S1A). This hydrogel preserves the channel's hydration, enabling high ionic conductivity while minimizing electronic conduction. The P(VDF-TrFE) μFbs layers with varying fiber diameters (1–3 μm) employ a screen-printed extraction electrode (Supplementary Fig. S1B). To complete the device, the channel/IM is coated with a thin layer of PEDOT:PSS and D-sorbitol mixture, serving as a conductive adhesive (CA)[45], and P(VDF-TrFE) μFbs layer is laminated on top (Supplementary Fig. S1C, D). The intermediate CA reduces the electrochemical impedance between the channel/IM and the μFb layer (Supplementary Fig. S4). Finally, the entire device is encapsulated without compromising the flexibility and elastic modulus of the μFbs film as described in materials and methods section.

Piezo-IGTs operate in depletion mode and have contain mobile ions within their conducting polymer channels that permit shorter ionic transit time. Upon application of mechanical stress, the piezoelectric P(VDF-TrFE) microfibers undergo deformation, shifting molecular dipoles and associated charge centers, resulting in electric polarization and the generation of voltage across the microfiber films (positive and negative signs) (Fig. 3A bottom). Under cyclic compression and decompression, the generated piezoelectric voltage alternates polarity. This alternating voltage attracts and repels mobile ions within the channel, causing repetitive doping and de-doping of the conducting polymer, ultimately leading to measurable fluctuations in the transistor's drain current (I_D) (Fig. 3A bottom). To gain insight into the operation mechanism and overall device performance, we first accessed the intermediate CA-based electrode and measured the output characteristics of the constituent IGT component (Fig. 3B inset). By varying the channel length (L) and the width-to-length ratio (W/L), we were able to optimize the device geometry to achieve maximum transconductance ($|g_m$max$| = 31.52$ mS) at a gate voltage (V_G) of approximately 0 V (Fig. 3B, Supplementary Figs. S2, S3 and S9). This allows the device to operate with the small input signal generated by μFbs close to maximum transconductance point without the need of externally applied V_G. Next, we investigated the whole device's response to mechanical stress by connecting the top electrode of P(VDF-TrFE) μFbs to Source (S) electrode and applying tapping deformations with varying weight (0.4 - 2.5 kPa) (Fig. 3C). Mechanical stress on the piezoelectric element causes deformation, which shifts molecular dipoles and charge centers, resulting in electric polarization and a voltage across the μFbs. This voltage attracts and repels the mobile ions within the device which they dope and de-dope the conducting polymer repetitively, leading to fluctuations in the drain current (I_D) of the transistor. A linear increase in applied pressure (from 0.4 to 2.5 kPa) led to an exponential rise in the piezoelectric response (Fig. 3C, black), where each incremental increase in weight results in a progressively larger difference in the normalized response. The maximum response was observed at approximately 2.5 kPa of applied pressure (Fig. 3C, red).

As the channel thickness of the constituent IGT component increases, the transconductance rises accordingly. This is attributed to the (de)doping processes occurring throughout the entire channel, leading to volumetric
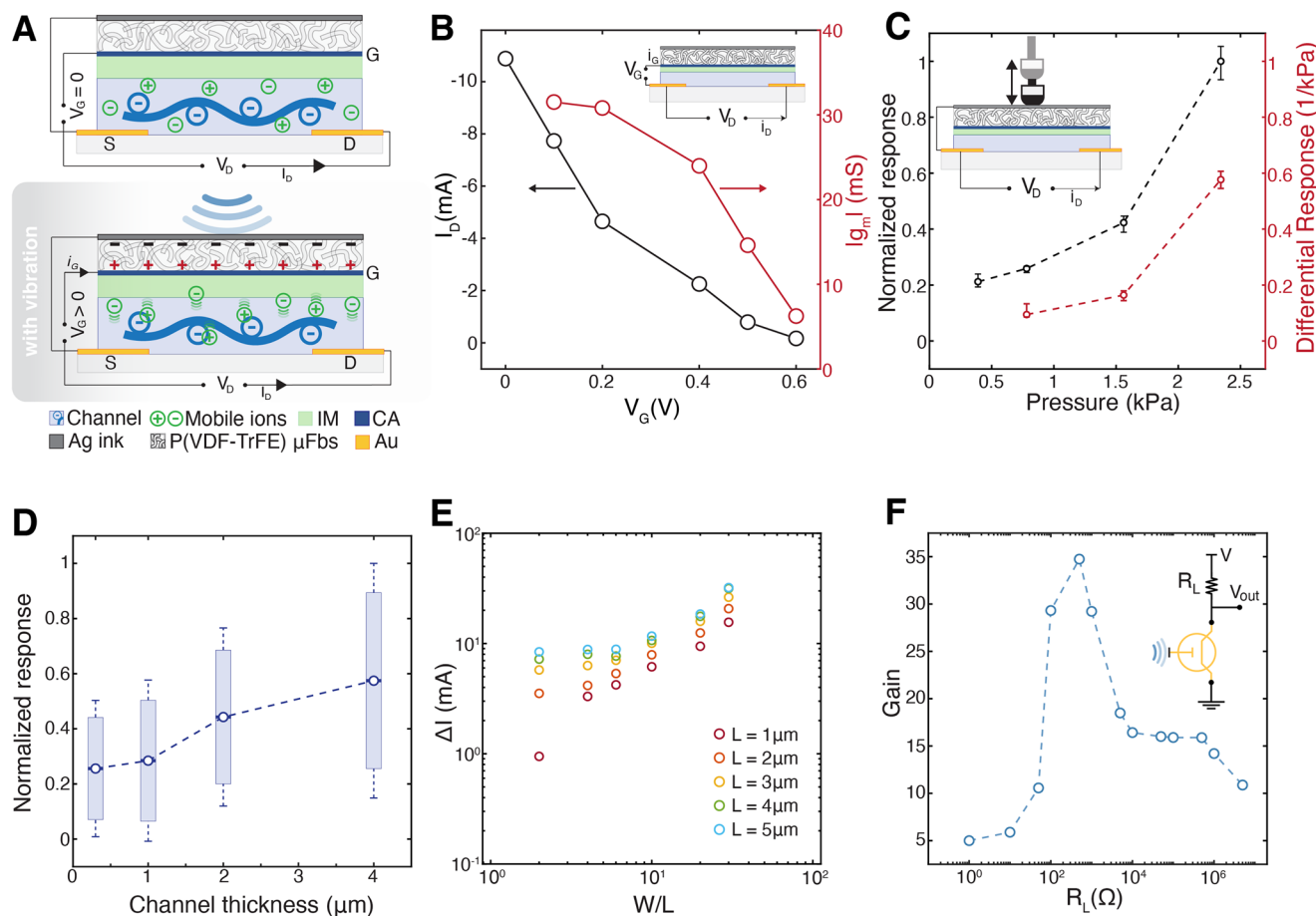
Fig. 3 | Piezo-IGT as an efficient piezoelectric transducer and amplifier.
A Schematic illustration of Piezo-IGT cross section and wiring diagram for device operation. The P(VDF-TrFE) µFb film laminated on the transistor channel via a conductive adhesive (CA; dark blue) captures mechanical stress, undergo deformation and generate voltage across the film (poisitive and negative signs) that induces (de)doping in the IGT channel through the ion membrane (green). G, S and D denote gate, source and drain terminals respectively. **B** Transfer curve (black) of the constituent IGT component (L = 5 µm, W = 150 µm, channel thickness; d = 2 µm) of a piezo-IGT, measured at $V_D = -0.6$ V, along with the corresponding transconductance (red), $|g_m max| = 31.52$ mS. Inset shows the wiring diagram. **C** Normalized drain current response of Piezo-IGTs (L = 5 µm, W/L = 30) to applied pressure (0.4–2.5 kPa). Inset shows a schematic illustration of the characterization setup using an Arduino-based tapping device. **D** Normalized drain current response of Piezo-IGTs as function of channel thickness. The mean current was calculated for 12 Piezo-IGTs with channel thicknesses ranging from 0.3 to 4 µm, while keeping the W/L ratio constant at 30 and channel length (L) at 5 µm. Measurements were taken at $V_D = -0.6$ V. **E** Piezoelectric transduction in a 5 × 6 array of Piezo-IGTs with increasing W/L ratios (2–30) and a constant channel thickness (d = 4 µm), all signals were recorded during 100 Hz tapping for $V_D = -0.6$ V. **F** Common-source amplifier configuration based on Piezo-IGT with load resistance varying from 1 to 5 MΩ and Piezo-IGT operating at V = −0.6 V. Maximum gain = 35.

capacitance. Consequently, with greater channel thickness, we observed an enhanced piezoelectric response in the Piezo-IGTs (Fig. 3D).

To better understand the impact of other geometrical parameters on device performance, we fabricated an array of Piezo-IGTs with a constant channel thickness of 4 µm, while varying the channel length (L = 1–5 µm) and width-to-length (W/L) ratios (W/L = 2–30) (Fig. 3E and Supplementary Fig. S1E, right). For the same W/L ratios, Piezo-IGTs with shorter channel lengths exhibited smaller ΔI values. This can be attributed to two factors: a smaller overlap area with the piezoelectric element and higher channel resistance (as increasing L increases the channel area for a given W/L ratio, thereby reducing channel resistance). For transistors with a channel length of L = 1 µm (Fig. 3E; dark red circles), ΔI values increased linearly with W/L ratios, indicating a direct relationship with transconductance (g_m)[46] (Fig. 3E and Supplementary Fig. S3). However, as the channel length increases, the relationship between ΔI and W/L deviates from linearity, suggesting that in smaller channel areas, factors such as overlap with the piezoelectric element and channel resistivity play a more dominant role.

Due to their high transconductance at $V_G \sim 0$ V and compatibility with scalable fabrication methods, Piezo-IGTs are ideal building blocks for mechanoresponsive and acousto-sensitive bioelectronics. They can easily be converted into common-source amplifiers by simply placing a resistor on the drain side without requiring additional gate biasing (Fig. 3F; inset). We supplied a Piezo-IGT (L = 5 µm, W/L = 30) with V = −0.6 V, where the output voltage (Vout) was directly influenced by the gate voltage (Vin) and the load resistor (R_L)[47]. The gain (Vout/Vin) increased proportionally with R_L up to 500Ω, where we observed a 35-fold increase in Vout, reaching 35 mV (Fig. 3F). However, as R_L increased further, the gain began to decrease, likely due to the decreases in V_D up to the point where transistor is not in the saturation regime. Moreover, amplification saturates for R_L values greater than 5 times the channel resistance ($R_L > 5*R_{chan}$)[47].

Piezo-IGTs enable vibration sensing with enhanced SNR
After investigating the channel properties, we analyzed the impact of µFbs fabrication conditions, specifically the electrospinning feed rate, on Piezo-IGT performance. By varying the feed rate from 3 to 6 ml/h, we controlled the mean diameter of the µFbs, which ranged from 1 to 3 µm. The piezoelectric response of Piezo-IGTs to mechanical stress increased with feed rates up to 5 ml/h, after which it declined (Fig. 4A). This trend is attributed to the effect of the feed rate on the electrospinning, leading to thicker films and larger fiber diameters at higher feed rates. Beyond 5 ml/h, fiber merging
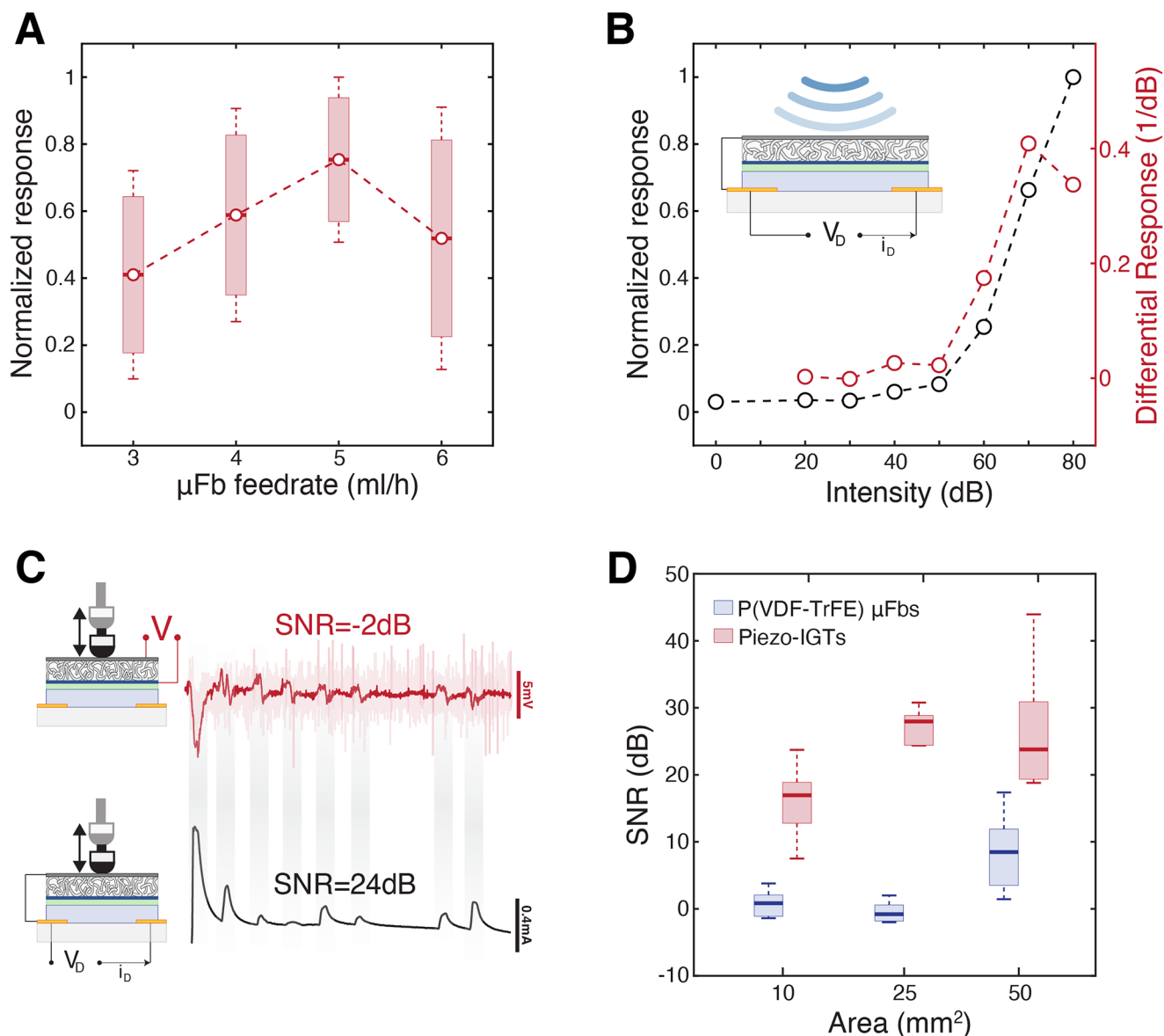
Fig. 4 | Piezo-IGTs enable vibration sensing with enhanced SNR. A Normalized drain current response of Piezo-IGTs as a function of P(VDF-TrFE) μFbs feed-rate. The mean current was calculated for 12 Piezo-IGTs (L = 5 μm, W/L = 30) with increasing μFbs feed rates (3–6 ml/h), while maintaining constant P(VDF-TrFE) film area (25 mm²) at V_D = -0.6 V. **B** Normalized drain current response of a Piezo-IGT device (L = 5 μm, W/L = 30) at various sound intensities. The maximum differential response was observed at 70 dB. **C** Piezo-IGTs showing enhanced SNR for piezoelectric signals. The signal generated by the P(VDF-TrFE) μFb layer had an initial SNR of −2 dB (red), which increased to 24 dB (black) after passing through the IGT. Light red trace depicts the voltage trace derived from P(VDF-TrFE) μFb film before notch filtering is applied. Gray shades indicate instances of taping deformations. **D** Statistical evaluation of SNR from 100 Hz tapping on 3 different μFb film areas (10, 25 and 50 mm²) used as a standalone film (blue) and as Piezo-IGT gates (red) at V_D = −0.6 V.

was observed, and the mean fiber diameter dropped to 1 μm, resulting in a decrease in piezoelectric response (Supplementary Fig. S7). We further monitored the response of Piezo-IGTs to varying sound intensities. Similar to mechanical stress response tests, Piezo-IGTs (L = 5 μm, W/L = 30) were exposed to a 100 Hz acoustic signal with sound intensities ranging from 0 to 80 dB. As sound intensity increased, the Piezo-IGTs exhibited an exponential increase in response, with the maximum differential response observed at 70 dB (Fig. 4B). Compared to stand-alone P(VDF-TrFE) μFb films, Piezo-IGTs not only amplified piezoelectric transduction but also produced higher-quality signals. The device architecture of Piezo-IGTs eliminates signal losses caused by impedance mismatch or resistance in transmission lines, allowing the original signal to be preserved and amplified early in the signal pathway, which significantly improves the SNR. Furthermore, the high gain-bandwidth product of the IGT enables it to respond to small input signals, producing large changes in the channel current[37,38].

This further boosts signal strength relative to noise, enhancing SNR. We simultaneously recorded the raw signal from the P(VDF-TrFE) μFb layer (Fig. 4C, top) and the amplified signal of piezo-IGT (Fig. 4C, bottom), clearly demonstrating the improved signal quality. The SNR of the Piezo-IGT signal was significantly higher at 24 dB, compared to the raw P(VDF-TrFE) μFb film of equal area, which had an SNR of −2 dB. Consequently, the characteristic peaks in the in the raw μFb film signal were only detectable after applying a notch filter between 40 and 60 Hz, whereas the signal acquired by the Piezo-IGT did not require such filtering. To further assess the SNR, we analyzed an array of Piezo-IGTs with varying μFb film gate areas (10 mm², 25 mm², and 50 mm²) and observed a consistent increase in SNR across all configurations (Fig. 4D).

To further evaluate the mechanical flexibility and functional sensitivity of the Piezo-IGTs, we conducted a series of controlled bending tests. Devices were bent repeatedly (5–30 cycles) around a 5 mm radius. After a slight
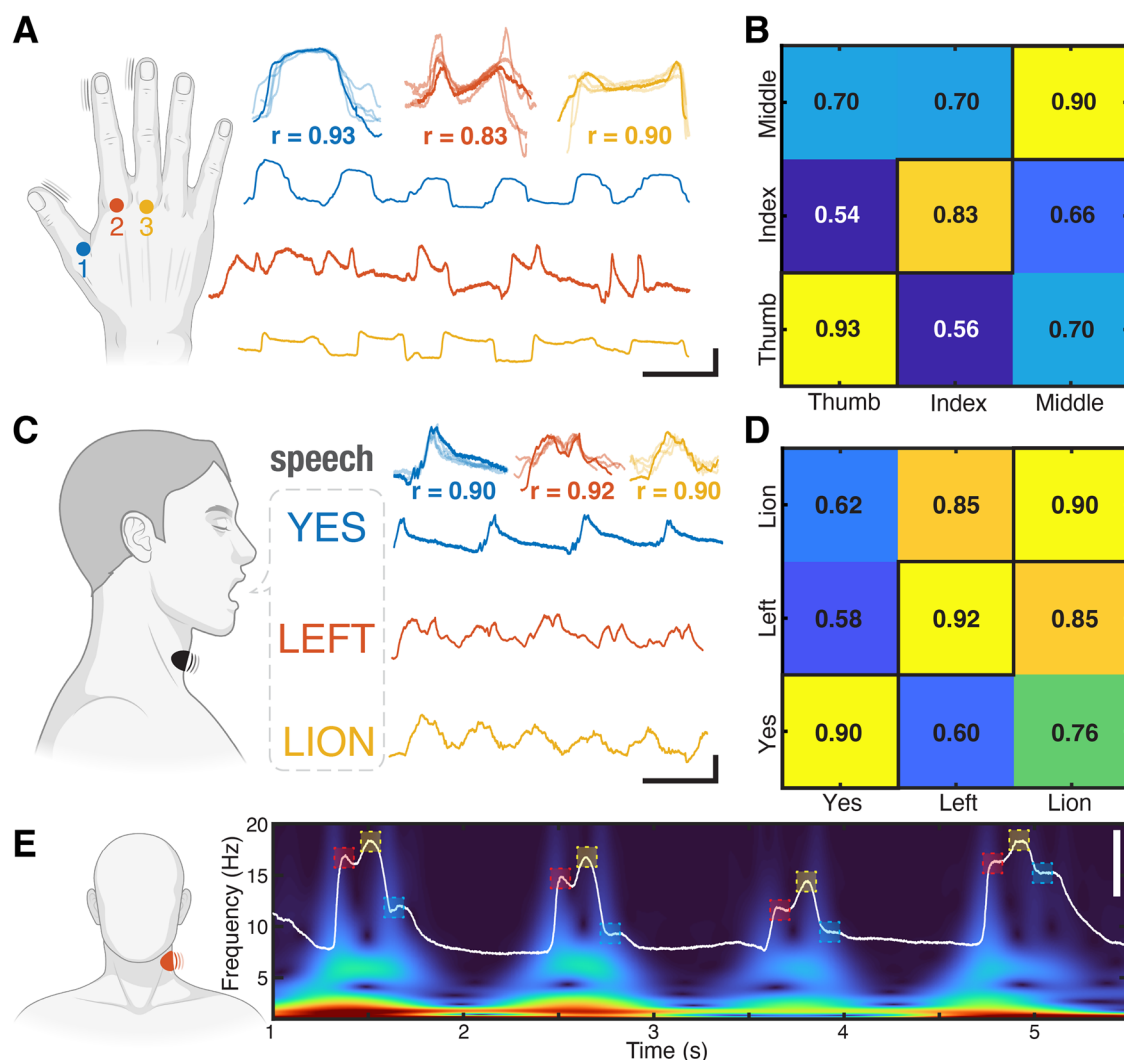
Fig. 5 | Piezo-IGTs acquire high-quality MMG, speech and MCG signals. A MMG recordings with distinct peaks, acquired from Piezo-IGTs placed on three different fingers: thumb (blue, 1), index (red, 2) and middle (yellow, 3). Bottom right: Sample traces of piezo-IGT acquired thumb movements (6 count, blue), index finger movements (5 counts, red), and middle finger movements (5 count, yellow). Top right: Autocorrelation of isolated waveforms representing the movement of each finger. Scale bar 1 s, 1 mA. **B** Cross-correlogram of the three piezo-IGT acquired MMG sample traces, highlighting the similarities in repeated movements across the different recordings. Each cell represents the correlation coefficients between movements of two fingers. **C** Piezo-IGTs used for speech recognition, generating distinct patterns for different spoken words ("Yes", "Left", and "Lion"). Bottom right: Sample traces of piezo-IGT acquired vocal vibrations when the words "Yes" (4 counts, blue), "Left" (5 counts, red), and "Lion" (5 counts, yellow) are spoken. Top right: Autocorrelation of isolated waveforms of vocal vibrations for each word. Scale bar 1 s, 3 mA. **D** Cross-correlogram of the piezo-IGT acquired vocal vibration from spoken words, showing maximum correlation coefficient for repeated signal of the same word. **E** Amplified MCG recording acquired with Piezo-IGT on the neck over the left carotid artery, along with the corresponding time-frequency spectrogram displaying the pulsatile blood flow during both systole and diastole of each heartbeat. Key features of the carotid waveform, including the anacrotic notch (red dashed square), dicrotic notch (blue dashed square) and systolic peaks (yellow dashed square) are clearly visible. White scale bar, 2 mA.

decline a progressive increase in the normalized piezoelectric response was observed with increasing cycle count, suggesting not only robust mechanical resilience but also a possible enhancement in performance possibly due to microstructural rearrangement or dipole alignment within the electrospun P(VDF-TrFE) μFbs (Supplementary Fig. S8A). Additionally, when bent across varying radii (2–10 mm), the devices retained stable and measurable output even at smaller radii (e.g. 2 mm), well within the typical curvature range of wearable applications (e.g., the human finger radius ~6–8 mm).

Piezo-IGTs acquire high-quality MMG, speech and MCG signals
The strong performance and versatility of Piezo-IGTs make them particularly well-suited for capturing physiological vibrations and body movements. We leveraged these capabilities to acquire high-quality signals through micro-scale Piezo-IGTs in mechanomyography (MMG), speech recognition, and mechanocardiography (MCG), demonstrating their

translational potential. Piezo-IGTs offer several advantages for recording physiological vibrations: (i) they eliminate the need for electrical referencing, (ii) enhance patient comfort by removing the requirement for ionic gels or additional interfaces with functional materials, (iii) enable high SNR signal acquisition within relevant frequency bands.

To validate their ability to capture high-quality physiological signals, we first tested Piezo-IGTs by recording MMG signals during three distinct finger movements. The encapsulated device was placed over the muscles controlling the thumb, index, and middle fingers. Piezo-IGTs successfully recorded distinct, high-quality signals corresponding to the consecutive movement of each finger, with each signal traceable back to the specific finger movement (Fig. 5A, Supplementary Fig. S11A). The cross-correlogram matrix of the MMG data quantifies the similarity between the waveforms of different finger movements (Fig. 5B). The higher correlation values along the diagonal indicate strong consistency in the Piezo-IGT

generated waveforms for repeated movements of the same finger, while the lower off-diagonal values highlight the differences between waveforms generated by different finger movements (Fig. 5B). These data support the notion that Piezo-IGTs can efficiently capture and differentiate small mechanical activity. To further highlight the enhanced performance of Piezo-IGTs, we recorded MMG from index finger using conventional bulk PVDF (blue) and P(VDF-TrFE) μFb (red) films. Both signals exhibited low SNR and required additional grounding and filtering to extract meaningful signal content (Supplementary Fig. S12). Next, we tested Piezo-IGTs for speech recognition by placing them on the anterior neck surface of a healthy volunteer. The volunteer repeated words such as "Yes", "Left", and "Lion" multiple times, and the Piezo-IGTs successfully generated distinct signal patterns for each spoken word. High correlation values were observed for repeated instances of the same word, demonstrating the reproducibility of the recorded signals (Fig. 5C, D). The cross-correlogram matrix further showed that while signals for different words are distinguishable, words with similar phonetic components (e.g. "Left" and "Lion") exhibited higher correlation values, reflecting the device's sensitivity to subtle vocal features (Fig. 5D).

Lastly, we recorded MCGs from the carotid artery of a healthy volunteer to assess the Piezo-IGT's ability to detect pressure variations resulting from blood flow dynamics. Positioned over the left carotid artery, the Piezo-IGT captured the pulsatile blood flow during both systole and diastole, reflecting the mechanical activity associated with each heartbeat (Fig. 5E, Supplementary Fig. S11B). The recorded pulse pressure waveforms displayed all the characteristic features of a healthy carotid arterial waveform, including the anacrotic and dicrotic limbs, their associated notches, a prominent systolic peak and the end of diastole point[48]. The anacrotic limb corresponds to the initial upstroke in arterial pressure during systole, where blood is rapidly ejected from the heart into the aorta. Notably, the anacrotic notch was observed, which results from the interaction of the forward pressure wave generated by the heart and the reflected wave returning from peripheral resistance within the arterial system. This feature is critical for assessing heart function and the elasticity of the blood vessels[49,50]. Following the systolic peak, the dicrotic limb was clearly visible as the waveform descended, reflecting the gradual decrease in pressure as the heart moves into diastole. The dicrotic notch was also distinctly captured, marking the closure of the aortic valve. This notch represents a brief period of backflow and is a key indicator of normal valve function and healthy arterial compliance (Fig. 5E). The corresponding time-frequency spectrogram of the pressure waveform reveals the higher-frequency components (10–20 Hz) coupled to the rapid rise in arterial pressure during systolic phase, and the lower-frequency components (5–10 Hz) connected to the slower pressure dynamics during diastolic phase (Fig. 5E).

Discussion

We developed a novel piezoelectric transistor architecture, the Piezo-IGT, which enables efficient transduction of small mechanical vibrations into amplified electrical signals. By combining one of the most advanced organic electrochemical transistor architectures to date (featuring a high gain-bandwidth product) with highly sensitive P(VDF-TrFE) μFb films, and leveraging advanced fabrication techniques, we achieved efficient and miniaturized architectures with channel lengths as small as L = 1 μm. Using P(VDF-TrFE) μFb films as laminated gate, we demonstrated that film deformation generates sufficient voltage to attract and repel ions in the polymeric channel. The constituent IGTs show high transconductance at approximately 0 V gate voltage ($V_G \sim 0$ V), ensuring that even small signals from the P(VDF-TrFE) μFb film are sufficient to drive the transistor close to its maximum transconductance without requiring external gate biasing. Compared to stand-alone P(VDF-TrFE) μFb films, Piezo-IGTs provide amplified piezoelectric transduction with significantly improved SNR, making them highly effective components for mechanoresponsive and acousto-sensitive bioelectronic circuits. While this study used PVDF-TrFE as a proof of concept, naturally occurring materials with piezoelectric

properties, such as chitosan, silk fibroin, and collagen, could be utilized as alternatives[51,52].

Piezo-IGTs were fabricated using sequential deposition and lamination techniques with biocompatible, readily available materials that can be easily processed and optimized through microfabrication and printing. The novel architecture of Piezo-IGTs eliminates signal losses caused by transmission line and impedance mismatch, preserving and amplifying the original signal early in the signal pathway. By tuning the properties of the channel and piezo films, the piezoelectric response of Piezo-IGTs can be tailored for specific applications. Furthermore, the compact and flexible structure of Piezo-IGTs, combined with the low-temperature fabrication processes employed, enables seamless integration into various conformable polymeric substrates without compromising device flexibility or piezoelectric performance. Although IGTs are stable in physiological environment, direct contact with biological tissues is not necessary for Piezo-IGTs. Therefore, additional encapsulation using a combination of parylene-C and atomic layer deposition could further enhance the long-term stability of the Piezo-IGTs in such environments.

We demonstrated the efficacy of Piezo-IGTs in acquiring high-quality physiological signals from MMG and MCG recordings, as well as speech recognition. Notably, this was achieved using micro-scale devices without requiring adhesive ionic gels and/or other functional materials, electrical referencing, or complex data acquisition systems. Piezo-IGTs locally amplified signals, successfully distinguishing between various types of vibrations and movements, further demonstrating precision and reliability in capturing mechanical activity. For speech recognition, Piezo-IGTs effectively differentiated distinct spoken words, highlighting their potential for advanced sensing applications.

These qualities make Piezo-IGTs ideal candidates for integration into bioelectronic circuits designed to interact with vibrations and movement. Our findings support their potential in application requiring precise detection and discrimination of small, localized mechanical signals, such as in prosthetics, gesture recognition, and speech recognition systems, without requiring additional signal processing. Piezo-IGTs could be employed in wearable devices and electronic skins, with promising applications in preventive health monitoring (e.g., sleep monitoring, seizure alerting systems), closed-loop therapeutic devices (e.g., for stabilizing Parkinson's disease symptoms), and even advanced cochlear implants that function without external components.

Methods

Microfiber fabrication

PVDF (52 μm) film was purchased from TE connectivity and P(VDF-TrFE) powder (F25) was purchased from Piezotech, France. 20 wt% of PVDF was added to 3:2 solution of dimethylformamide (DMF) and acetone and stirred at 500 rpm until fully dissolved. The polymer solution was then transferred to a 20 ml syringe and connected to a 21-gauge steel needle via a polytetrafluoroethylene (PTFE) tube. The syringe was mounted on a pump with the needle being inserted into the custom-built electrospinning machine. A static 15 kV DC voltage was applied between the needle and the collector. The distance between the needle and the collector was maintained at 15 cm. The feed rate was varied between 3–6 ml/h to investigate its effect. Electrospinning was carried out at room temperature (22–25 °C) in a laboratory with a central ventilation system and a dehumidifier. The electrospun films were collected on an A4 paper, peeled off, and cut into desired diameters using a blade. The films were then coated with electrode materials on both sides to enable charge extraction. Stand-alone films were laminated with polyimide (PI) for environmental isolation (Supplementary Fig. S1A–C).

IGT fabrication

PEDOT:PSS (Clevios PH1000) was obtained from Heraeus. D-Sorbitol, (3-glycidyloxypropyl)trimethoxysilane (GOPS), 4-dodecyl benzene sulfonic acid (DBSA), chitosan (low molecular weight), Glycerol, Micro 90 and 3-(trimethoxysilyl)propyl methacrylate (A-174 silane) were purchased from Sigma Aldrich. AZnLOF2020 (negative photoresist), AZ10xT (positive

photoresist), AZ 400 K, AZ 726 MIF (metal ion free) developers and TechniStripp Ni555 (stripper) were acquired from MicroChemicals.

Cleaned 4" silicon wafers were coated with a 2-μm-thick parylene layer, which provided a conformable substrate. The Au electrodes and interconnects were patterned via photolithography and lift-off processes. AZnLOF2020 was spin-coated (3000 rpm), baked on a hot plate at 110 °C, exposed using a Suss MA6 Mask Aligner, and developed with AZ 726 MIF developer. Ti (10 nm) and Au (150 nm) layers were deposited with an e-beam metal evaporator. Lift-off was performed by immersing the substrates in a bath with TechniStripp Ni555. To electrically isolate the Au electrodes, an additional 2 μm parylene layer was coated on the samples, with adhesion enhanced by applying 3-(trimethoxysilyl)propyl methacrylate (A-174 silane) during coating. Then 5% of micro 90 in DI water was spin coated to form an anti-adhesive layer. A sacrificial third parylene layer (2 μm) was deposited on top. AZ10xT was spin-coated (2000rpm), baked at 110 °C, exposed using a Suss MA6 Mask Aligner, and developed with AZ400K developer. The areas that corresponded to IGT channel and contact pads were etched via successive photolithography and reactive ion etching steps [Advanced Vacuum Vision 320; 140 W, 50-sccm (standard cubic centimeters per minute) O_2, and 5-sccm SF_6]. To realize the transistor channels, we spin-coated a mixture of PEDOT:PSS with d-sorbitol [40% d-sorbitol, 1% GOPS (as a cross-linker), and 0.1% DBSA (to improve film processing and wettability)] and patterned it by peeling off the third parylene layer (Supplementary Fig. S1A). To realize the ionic membrane, a solution of 20% chitosan (in acetic acid) and glycerol was spin coated on the IGT channel and annealed at 80 °C for 10 min to form an electrolyte hydrogel. Lastly, the channel is coated with a thin layer of PEDOT:PSS: D-sorbitol mixture, serving as a conductive adhesive (CA) to aid integration with P(VDF-TrFE) μFb film (Supplementary Fig. S1A).

Piezo-IGTs fabrication
To fabricate a Piezo-IGT, the P(VDF-TrFE) μFb film was integrated with IGT. The μFb film acted as a gate to the IGT. Top side of the film was screen printed with Ag ink while bottom side was laminated on the CA coated on the IGT channel, and annealed at 80 °C for 5 min to ensure good contact. The Ag side of the PVDF film was shorted with the source of the IGT. The device was then sealed with PI to preserve the channel hydration and to ensure environmental isolation (Supplementary Fig. S1C–E).

Electrical characterization
Voltage-time measurements were recorded from the Siglent SDS1204X-E 200 MHz Four channel oscilloscope, while current-voltage characteristics were measured with a Keysight B2902A Precision Source/Measurement Unit using two channels. On the first channel (V_D), linear sweeps from 0 V to −0.6 V were performed. On the second channel (V_G), constant voltages from 0 to 0.6 V were applied to the gate. The electrical characteristics of Piezo-IGTs were measured with Chitosan: Glycerol hydrogel as an electrolyte and P(VDF-TrFE) μFb film as gate electrode. Temporal response of Piezo-IGTs was also recorded with Keysight B2902A Precision Source/Measurement Unit using only one channel, with constant V_D at −0.6 V (saturation regime). No external V_G was applied. The device responded to the taps of 100 Hz from the tapping machine. The tapping machine was made in lab and comprised of servo motor and a potentiometer operated via Arduino. The sound measurements were performed by immersing the device inside the water bath with a speaker. A reference microphone was used to measure the sound intensities. While Voltage-Time response of Piezo-IGT and standalone PVDF films, were recorded via Siglent Oscilloscope Electrochemical impedance spectroscopy was performed with PalmSens4 with P(VDF-TrFE) μFb film acting as working electrode and source of Piezo-IGT as counter and reference electrode. Lastly, we acquired scanning electron microscopy (SEM) images of μFb films with FEI Nova 600 Nanolab Dual-Beam FIB-SEM.

MCG, MMG and speech recordings
All recordings were performed on a healthy volunteer. During recording, Piezo-IGT operated at $V_D = -0.6$ V. Piezo-IGT was placed on the carotid artery to acquire MCG signal. For MMG, the volunteer was asked to perform specific movements of hands and fingers to isolate targeted muscles. The movements of specific fingers were recorded by placing the device on Lumbricalis muscles. For speech recognition, the Piezo-IGT was affixed to the anterior neck surface midway between the thyroid prominence and the suprasternal notch. The volunteer was asked to repeat specific words several times. All the measurements were recorded with a Keysight B2902A Precision Source/Measurement and data were stored for off-line analysis with a 16-bit format, analyzed using MATLAB (MathWorks).

Data availability
All data supporting the conclusions of the paper are available in the paper and/or the Supplementary Information. Additional data related to this paper may be requested from the authors.

References
1. Buzsáki, G., Anastassiou, C. A. & Koch, C. The origin of extracellular fields and currents — EEG, ECoG, LFP and spikes. *Nat. Rev. Neurosci.* **13**, 407–420 (2012).
2. Hodaie, M., Wennberg, R. A., Dostrovsky, J. O. & Lozano, A. M. Chronic Anterior Thalamus Stimulation for Intractable Epilepsy. *Epilepsia* **43**, 603–608 (2002).
3. Wilson, B. S. Cochlear implants: Current designs and future possibilities. *J. Rehabilit. Res. Dev.* **45**, 695–730 (2008).
4. Wong, K. et al. Auditory Brainstem Implants: Recent Progress and Future Perspectives. *Front. Neurosci.* **13** https://doi.org/10.3389/fnins.2019.00010 (2019).
5. Fan, X. et al. Ultrathin, Rollable, Paper-Based Triboelectric Nanogenerator for Acoustic Energy Harvesting and Self-Powered Sound Recording. *ACS Nano* **9**, 4236–4243 (2015).
6. Jung, Y., Kwak, J.-H., Lee, Y., Kim, W. & Hur, S. Development of a Multi-Channel Piezoelectric Acoustic Sensor Based on an Artificial Basilar Membrane. *Sensors* **14**, 117–128 (2013).
7. Lee, H. S. et al. Flexible Inorganic Piezoelectric Acoustic Nanosensors for Biomimetic Artificial Hair Cells. *Adv. Funct. Mater.* **24**, 6914–6921 (2014).
8. Roy, K. et al. A Self-Powered Wearable Pressure Sensor and Pyroelectric Breathing Sensor Based on GO Interfaced PVDF Nanofibers. *ACS Appl. Nano Mater.* **2**, 2013–2025 (2019).
9. Wang, C. et al. Tissue-Adhesive Piezoelectric Soft Sensor for In Vivo Blood Pressure Monitoring During Surgical Operation. *Adv. Functional Mater.* **33** https://doi.org/10.1002/adfm.202303696 (2023).
10. Schwartz, G. et al. Flexible polymer transistors with high pressure sensitivity for application in electronic skin and health monitoring. *Nat. Commun.* **4**, 1859–1859 (2013).
11. Zhao, C., Park, J., Root, S. E. & Bao, Z. Skin-inspired soft bioelectronic materials, devices and systems. *Nat. Rev. Bioeng.* **2**, 671–690 (2024).
12. Khodagholy, D. et al. In vivo recordings of brain activity using organic transistors. *Nat. Commun.* **4**, 1575–1575 (2013).
13. Drakopoulou, S. et al. Hybrid neuroelectronics: towards a solution-centric way of thinking about complex problems in neurostimulation tools. *Front. Electronics* **4** https://doi.org/10.3389/felec.2023.1250655 (2023).
14. Aabid, A. et al. A Systematic Review of Piezoelectric Materials and Energy Harvesters for Industrial Applications. *Sensors* **21**, 4145–4145 (2021).
15. Jiang, C. et al. All-electrospun flexible triboelectric nanogenerator based on metallic MXene nanosheets. *Nano Energy* **59**, 268–276 (2019).
16. İlik, B., Koyuncuoğlu, A., Şardan-Sukas, Ö. & Külah, H. Thin film piezoelectric acoustic transducer for fully implantable cochlear implants. *Sens. Actuators A Phys.* **280**, 38–46 (2018).

17. Inaoka, T. et al. Piezoelectric materials mimic the function of the cochlear sensory epithelium. *Proc. Natl Acad. Sci.* **108**, 18390–18395 (2011).

18. Zaszczyńska, A., Gradys, A. & Sajkiewicz, P. Progress in the Applications of Smart Piezoelectric Materials for Medical Devices. *Polymers* **12**, 2754–2754 (2020).

19. Viola, G. et al. Bioinspired Multiresonant Acoustic Devices Based on Electrospun Piezoelectric Polymeric Nanofibers. *ACS Appl. Mater. Interfaces* **12**, 34643–34657 (2020).

20. Zhang, D. et al. Enhanced piezoelectric performance of PVDF/BiCl3/ZnO nanofiber-based piezoelectric nanogenerator. *Eur. Polym. J.* **166**, 110956–110956 (2022).

21. Stadlober, B., Zirkl, M. & Irimia-Vladu, M. Route towards sustainable smart sensors: ferroelectric polyvinylidene fluoride-based materials and their integration in flexible electronics. *Chem. Soc. Rev.* **48**, 1787–1825 (2019).

22. Chen, F. et al. Effect of stretching orientation on the crystalline structure and energy storage properties of poly(vinylidene fluoride) films. *Mater. Today Commun.* **41**, 110598–110598 (2024).

23. Motamedi, A. S., Mirzadeh, H., Hajiesmaeilbaigi, F., Bagheri-Khoulenjani, S. & Shokrgozar, M. Effect of electrospinning parameters on morphological properties of PVDF nanofibrous scaffolds. *Prog. Biomater.* **6**, 113–123 (2017).

24. Ico, G. et al. Size-dependent piezoelectric and mechanical properties of electrospun P(VDF-TrFE) nanofibers for enhanced energy harvesting. *J. Mater. Chem. A* **4**, 2293–2304 (2016).

25. Wang, X. et al. Tactile-Sensing Based on Flexible PVDF Nanofibers via Electrospinning: A Review. *Sensors* **18**, 330–330 (2018).

26. Chen, D., Wang, C., Chen, W., Chen, Y. & Zhang, J. X. J. PVDF-Nafion nanomembranes coated microneedles for in vivo transcutaneous implantable glucose sensing. *Biosens. Bioelectron.* **74**, 1047–1052 (2015).

27. Li, T. et al. Pure OPM nanofibers with high piezoelectricity designed for energy harvesting in vitro and in vivo. *J. Mater. Chem. B* **6**, 5343–5352 (2018).

28. Pan, C.-T. et al. Development of MMG sensors using PVDF piezoelectric electrospinning for lower limb rehabilitation exoskeleton. *Sens. Actuators A Phys.* **301**, 111708–111708 (2020).

29. Xin, Y. et al. Flexible piezoelectric sensor based on PVDF-TrFE/Nanoclay composite nanofibers for physiological micro-vibration signal sensing. *Measurement* **201**, 111742–111742 (2022).

30. Li, G.-Y. et al. Hierarchical PVDF-HFP/ZnO composite nanofiber–based highly sensitive piezoelectric sensor for wireless workout monitoring. *Adv. Compos. Hybrid. Mater.* **5**, 766–775 (2022).

31. Rivnay, J., Wang, H., Fenno, L., Deisseroth, K. & Malliaras, G. G. Next-generation probes, particles, and proteins for neural interfacing. *Sci. Adv.* **3** https://doi.org/10.1126/sciadv.1601649 (2017).

32. Ohayon, D., Druet, V. & Inal, S. A guide for the characterization of organic electrochemical transistors and channel materials. *Chem. Soc. Rev.* **52**, 1001–1023 (2023).

33. Nawaz, A., Liu, Q., Leong, W. L., Fairfull-Smith, K. E. & Sonar, P. Organic Electrochemical Transistors for In Vivo Bioelectronics. *Adv. Mater.* **33** https://doi.org/10.1002/adma.202101874 (2021).

34. Rivnay, J. et al. Organic electrochemical transistors. *Nat. Rev. Mater.* **3**, 17086–17086 (2018).

35. Makhinia, A., Beni, V. & Andersson Ersman, P. Screen-Printed Piezoelectric Sensors on Tattoo Paper Combined with All-Printed High-Performance Organic Electrochemical Transistors for Electrophysiological Signal Monitoring. *ACS Appl. Mater. Interfaces* **16**, 61428–61434 (2024).

36. Shintaku, H., Inaoka, T., Nakagawa, T., Kawano, S. & Ito, J. Electrically Evoked Auditory Brainstem Response by Using Bionic Auditory Membrane in Guinea Pigs. *J. Biomech. Sci. Eng.* **8**, 198–208 (2013).

37. Cea, C. et al. Enhancement-mode ion-based transistor as a comprehensive interface and real-time processing unit for in vivo electrophysiology. *Nat. Mater.* **19**, 679–686 (2020).

38. Spyropoulos, G. D., Gelinas, J. N. & Khodagholy, D. Internal ion-gated organic electrochemical transistor: A building block for integrated bioelectronics. *Sci. Adv.* **5** https://doi.org/10.1126/sciadv.aau7378 (2019).

39. Mai, M., Ke, S., Lin, P. & Zeng, X. Ferroelectric Polymer Thin Films for Organic Electronics. *J. Nanomater.* **2015** https://doi.org/10.1155/2015/812538 (2015).

40. Shao, H., Fang, J., Wang, H. & Lin, T. Effect of electrospinning parameters and polymer concentrations on mechanical-to-electrical energy conversion of randomly-oriented electrospun poly(vinylidene fluoride) nanofiber mats. *RSC Adv.* **5**, 14345–14350 (2015).

41. Ruggero, M. A. Cochlear Delays and Traveling Waves: Comments on 'Experimental Look at Cochlear Mechanics': [A. Dancer, Audiology 1992;31:301-312]. *Int. J. Audiol.* **33**, 131–142 (1994).

42. Lepak-Kuc, S. et al. Low-temperature silver-based ink for highly conductive paths through industrial printing processes suitable for thermally sensitive substrates and beyond. *J. Mater. Res.* **39**, 297–310 (2024).

43. Idris, M. K. & Grau, G. Dispense Printing of Silver Flake Inks on Hydrophilic and Hydrophobic Surfaces. *Adv. Eng. Mater.* **26** https://doi.org/10.1002/adem.202401302 (2024).

44. Sharova, A. S. et al. Chitosan-gated organic transistors printed on ethyl cellulose as a versatile platform for edible electronics and bioelectronics. *Nanoscale* **15**, 10808–10819 (2023).

45. Spyropoulos, G. D. et al. Organic and perovskite solar modules innovated by adhesive top electrode and depth-resolved laser patterning. *Energy Environ. Sci.* **9**, 2302–2313 (2016).

46. Friedlein, J. T., McLeod, R. R. & Rivnay, J. Device physics of organic electrochemical transistors. *Org. Electron.* **63**, 398–414 (2018).

47. Braendlein, M., Lonjaret, T., Leleux, P., Badier, J. M. & Malliaras, G. G. Voltage Amplifier Based on Organic Electrochemical Transistor. *Adv. Sci.* **4** https://doi.org/10.1002/advs.201600247 (2017).

48. O'Rourke, M. F., Pauca, A. & Jiang, X. J. Pulse wave analysis. *Br. J. Clin. Pharmacol.* **51**, 507–522 (2001).

49. Mulder, M. P. et al. Distinct morphologies of arterial waveforms reveal preload-, contractility-, and afterload-deficient hemodynamic instability: An in silico simulation study. *Physiological Rep.* **10** https://doi.org/10.14814/phy2.15242 (2022).

50. Mitchell, G. F. Arterial stiffness and wave reflection: Biomarkers of cardiovascular risk. *Artery Res.* **3**, 56–56 (2009).

51. Wu, Y. et al. From electricity to vitality: the emerging use of piezoelectric materials in tissue regeneration. *Burns Trauma* **12** https://doi.org/10.1093/burnst/tkae013 (2024).

52. Yue, X. et al. Silk fibroin-based piezoelectric nanofibrous scaffolds for rapid wound healing. *Biomater. Sci.* **11**, 5232–5239 (2023).

Acknowledgements

Author contributions

G.D.S., L.S., and T.L.C. conceived the project. G.D.S., L.S., S.D. designed, developed, fabricated and characterized the materials and devices. G.D.S., L.S., S.D. performed MMG, speech recognition and MCG recordings. All authors contributed to writing the paper.

Competing interests

The authors declare no competing interests.

Additional information